

RSC Advances



This is an *Accepted Manuscript*, which has been through the Royal Society of Chemistry peer review process and has been accepted for publication.

Accepted Manuscripts are published online shortly after acceptance, before technical editing, formatting and proof reading. Using this free service, authors can make their results available to the community, in citable form, before we publish the edited article. This *Accepted Manuscript* will be replaced by the edited, formatted and paginated article as soon as this is available.

You can find more information about *Accepted Manuscripts* in the [Information for Authors](#).

Please note that technical editing may introduce minor changes to the text and/or graphics, which may alter content. The journal's standard [Terms & Conditions](#) and the [Ethical guidelines](#) still apply. In no event shall the Royal Society of Chemistry be held responsible for any errors or omissions in this *Accepted Manuscript* or any consequences arising from the use of any information it contains.

Cite this: DOI: 10.1039/c0xx00000x

www.rsc.org/xxxxxx

ARTICLE TYPE

Size-controlled porous superparamagnetic $\text{Zn}_{1/3}\text{Fe}_{8/3}\text{O}_4$ nanospheres: synthesis, properties and application for drug delivery

Shengping Gao,^a Changyu Wu,^a Hui Jiang,^a Donghua Chen,^a Qiwei Li,^a Xiaoli Liu,^a Xuemei Wang^{*a}

Received (in XXX, XXX) Xth XXXXXXXXX 20XX, Accepted Xth XXXXXXXXX 20XX

DOI: 10.1039/b000000x

Abstract: Magnetic nanospheres have recently attracted much attention in the biomedical areas due to their good biocompatibility and unique magnetic features. Herein we report the synthesis and characterization of different sized porous superparamagnetic iron oxide nanospheres (SPION) ($\text{Zn}_{1/3}\text{Fe}_{8/3}\text{O}_4$) which are based on a new rational method of elevated-temperature hydrolysis of chelate iron alkoxide complexes in solutions of corresponding alcohol, diethyleneglycol (DEG) and diethanolamine (DEA). The size of the SPION is controlled by changing the ratio of the reaction media. It is noted that the highly water dispersible porous SPION with narrow size distribution can be tuned from 6.5 to 200 nm, each of which is composed of many single magnetite crystallites with approximately 5.5 nm in size. The SPION show superparamagnetic properties at room temperature. The superparamagnetic behavior, high magnetization, and high water dispersibility make these nanospheres ideal candidates for various important applications for drug delivery.

1. Introduction

The synthesis of functional nanospheres with controllable size is of great importance because of their fundamental scientific significance and broad technological applications. Magnetic nanospheres with good biocompatibility have attracted much attention in the past few decades owing to their unique magnetic features and important applications in biomedicine and bioimaging^{1,2}. Today, porous superparamagnetic iron oxide nanospheres (SPION) have received great attention for their superior characteristics such as controllable size, low toxicity, high liquid dispersibility, unique magnetic responsibility, high saturation magnetization values, functional modification and their easy manipulation with low magnetic fields. Because of their unique physical and chemical properties, they have been used in various areas of biotechnology and biomedicine including immuno-assays³, cell separation⁴, proteomics⁵, purification or detection of proteins⁶, DNA⁷, targeted drug delivery^{8,9}, magnetic resonance imaging¹⁰.

The structured cubic spinel $\text{M}_x\text{Fe}_{3-x}\text{O}_4$ represents an important class of iron oxide magnetic materials where oxygen forms a close packing, and M^{2+} and Fe^{3+} occupy either tetrahedral or octahedral interstitial sites. By adjusting the chemical identity of M^{2+} , the magnetic configurations of $\text{M}_x\text{Fe}_{3-x}\text{O}_4$ can be molecularly engineered to provide a wide range of magnetic properties. Due in part to this versatility, nanometer-scale $\text{M}_x\text{Fe}_{3-x}\text{O}_4$ superparamagnetic materials have been among the most frequently chosen systems for studies of nanomagnetism and have shown great potential for above applications¹¹. Wen et al reported for the first time that the samples of $\text{Zn}_x\text{Fe}_{3-x}\text{O}_4$ appear unusual maximal saturation magnetization when the amount of

Zn doped into Fe_3O_4 is up to 1/3¹². The synthesis of superparamagnetic nanospheres with controlled size has long been of scientific and technological interest. The size of the nanospheres is one of the important parameters influencing magnetic properties and is the key for the biological applications. Magnetic nanospheres with diameters less than 20 nm are believed to be superparamagnetic because they do not have a sufficient volume ensure a stable magnetic moment. This superparamagnetism, unique to nanospheres, is very important for their use as drug delivery vehicles and magnetic resonance imaging because these nanospheres have good biological compatibility and the influence on the sample *in vivo* can be kept to a minimum¹³, which can facilitate to literally drag drug molecules to their target site in the body under the influence of an applied magnetic field. Moreover, once the applied magnetic field is removed, the magnetic nanospheres retain no residual magnetism at room temperature and hence are unlikely of agglomerating (i.e., they are easily dispersed), thus evading uptake by phagocytes and increasing their half-life in the circulation. Moreover, due to a negligible tendency to agglomerate, SPION pose no danger of thrombosis or blockage of blood capillaries¹⁴. Nanospheres with sizes smaller than 10 nm are mainly removed by renal clearance, whereas nanospheres larger than 200 nm become concentrated in the spleen or are taken up by phagocytic cells of the body, in both instances leading to decreased plasma concentrations. Nanospheres with a size range of 5–200 nm are considered to be optimum, with longer circulation times because they can easily escape from recognition by the reticuloendothelial. They are also able to penetrate through very small capillaries¹⁵.

In this study, we report a novel approach to achieve size-controlled porous SPION ($\text{Zn}_{1/3}\text{Fe}_{8/3}\text{O}_4$) that could be adjusted by

changing the ratio of the reaction media. It is noted that the highly water dispersible SPION with narrow size distribution can be tuned from 6.5 to 200 nm, each of which is composed of many single magnetite crystallites approximately 5.5 nm in size. The nanospheres show superparamagnetic properties at room temperature, where the single crystalline magnetite particles within the same size range exhibit ferromagnetic behavior. The superparamagnetic behavior, high magnetization and high water dispersibility make these nanospheres ideal candidates for various important applications for drug delivery¹⁶.

2. Experimental Section

2.1. Materials

All reagents of analytical grade purity were purchased from Shanghai Chemical Reagents Co. and used without further purification. The ethanol was redistilled with the traditional Mg-I₂ system to increase the purity above 99.95%. The phosphate buffer solution (PBS, 0.1 M, pH 7.4) was prepared by using double distilled water (Millipore Ltd. USA).

2.2. Synthesis of the superparamagnetic iron oxide nanospheres (Zn_{1/3}Fe_{8/3}O₄)

Initially, 0.7 mmol ZnCl₂, 1.3 mmol FeCl₂ · 4H₂O and 4mmol of FeCl₃ · 6H₂O were dissolved in diethyleneglycol (DEG) or a mixture of DEG and diethanolamine (DEA) (4:1, 2:1, 1:1, v/v) in a flask under protection with nitrogen gas, respectively. Meanwhile, 16 mmol of NaOH was dissolved in DEG or a mixture of DEG and DEA (4:1, 2:1, 1:1, v/v). Then the solution of NaOH was added to a solution of metal chlorides with stirring at room temperature, causing an immediate color change from bright yellow to deep green-brown. After reaction for 1 h, the temperature of the solution was raised to 200°C and then kept constant for 8 h in the temperature of 200 °C in an autoclave. The solid product was isolated by cooling the reaction mixture to room temperature and centrifuging. A black solid was obtained and washed with ethanol twice and a mixture of ethanol and ethylacetate (1:1, v/v) three times to remove the excess of DEG and DEA. The detailed experimental data are listed in Table 1.

2.3. Characterization of SPION

The transmission electron microscope (TEM) images were obtained on a JEM-2100 transmission electron microscope operating at 200 kV. The sample morphology was evaluated by scanning electron microscopy (SEM, JEOL JSM-5900). The particle size distributions using Dynamic Light Scattering and zeta potential was measured by using a Zetasizer NanoZS size analyzer (ZS90, Malvern, UK). The crystalline phase was determined by powder X-ray diffraction (XRD) pattern (Bruker D8, Cu-Kα radiation) obtained on a DMAX-B (Rigaku Denki Corp., Tokyo, Japan). The fluorescence, absorption spectroscopy and Fourier-transformed infrared (FT-IR) spectroscopy study were performed on a Hitachi F-7000 fluorescence spectrophotometer, a HITACHI U-4100 ultraviolet spectrophotometer, and a Thermo Nicolet Avatar 360 FT-IR spectrophotometer, respectively.

2.4. Preparation of drug-loaded porous SPION

Initially, 20 mg of porous SPION and 20 mg of Doxorubicin (DOX) base were mixed in 4 mL of ethanol solution and stirred for 2 h. Then 6 mL of water was added dropwise into the suspension with stirring. The suspension was stirred for 4 h until the ethanol had evaporated. The drug loaded porous SPION were collected by magnetic separation and finally dispersed in PBS buffer (pH=7.4). The samples were ultra-centrifuged at 14000 rpm for 10 min. The DOX concentration in the supernatant was measured using a standard DOX concentration curve calibrated by a series of DOX solutions with different concentrations at the wavelength of 480 nm on a UV-Vis spectrophotometer.

The DOX loading capacity of Zn_{1/3}Fe_{8/3}O₄ was calculated according to the following formula¹⁷:

$$\text{Drug loading capacity}\% = (W_1 - W_2) / W \times 100\%$$

$$\text{Encapsulation efficiency}\% = (W_1 - W_2) / W_1 \times 100\%$$

Where W₁ is the initial weight of the drug for loading, W₂ is the residual weight of drug in solution after being loaded onto Zn_{1/3}Fe_{8/3}O₄, and W is the weight of Zn_{1/3}Fe_{8/3}O₄ for loading, respectively.

2.5. Cell culture

HepG2 hepatoma cells (Shanghai Institutes for Biological Sciences, Chinese Academy of Sciences) were maintained in DMEM/High glucose medium containing 10% fetal bovine serum and antibiotics (100 mg/mL streptomycin and 100 IU/mL penicillin) at 37 °C in a CO₂ incubator.

2.6. In vitro cytotoxicity studies of the SPION and the drug-loaded SPION

The cell viability was measured by the MTT method. HepG2 cells were seeded in 96-well plates at a concentration of 1.0×10⁴ cells/well, and incubated overnight at 37 °C in a 5% CO₂ humidified environment. Then the cells were separately treated with different sized drug-loaded SPION. The final concentration of DOX in each well of the HepG2 cells were treated with a final concentration of 0, 10.0, 20.0, and 40.0 μg/mL (dissolved with DMEM/High glucose medium), separately. The control groups were cultivated under the same condition without DOX and nanospheres. After all samples were cultured for 48 h, 20 μL of 5 mg/mL MTT (3-(4, 5-dimethylthiazol-2-yl)-2, 5-diphenyltetrazolium bromide) was added and incubated for additional 4 h. Subsequently, the plate was centrifuged at 1000 rpm for 10 min and the supernatant was discarded, followed by addition of 150 μL of DMSO into each well and gently shaking in the shaker incubator at 37 °C for 10 min. After this, the optical density (OD) at 492 nm was recorded. The cell viability was expressed as follows:

$$\text{Cell viability} (\%) = [A]_{\text{test}} / [A]_{\text{control}} \times 100\%$$

Where [A] represents the absorbance value at 492 nm. Each experiment was repeated at least three times.

2.7. Statistics

Data were expressed as the means ± SD (standard deviation) from at least three independent experiments. One-tailed unpaired

Student's t-test was used for significance testing, and $p < 0.05$ is considered significant.

3. Results and Discussion

3.1. TEM/SEM images and XRD patterns of the different sized porous SPION

Typical TEM images demonstrate that the size of the corresponding SPION can be precisely controlled from about 6.0 to about 200.0 nm by simply changing the ratio of the reaction medium (DEG and DEA) while keeping all other parameters fixed, as shown in Table 1. The structure of porous SPION can be also observed clearly in Fig. 1 (a~d). SEM images (Fig. 1 (a2~d2)) clearly show that the SPION are composed of small primary crystals with a size of 5.2–6.4 nm and the same crystal orientation. It can be seen that the porous SPION have different sizes (diameters of ca. 6.4, 39.0, 74.0 and 191.0 nm). Porous SPION size distributions of the samples in H₂O measured by dynamic light scattering (Fig. 1 (a1~d1)) illustrate that the porous SPION sizes of the samples are relatively narrow and the sizes are identical to those observed by SEM and TEM, suggesting that there exists almost no particle agglomeration or swelling in H₂O. The X-ray diffraction (XRD) measurements and Energy Dispersive Spectroscopy (EDS) about sample a (6.4nm) also confirm the structure of SPION. Fig. 2 shows diffraction patterns with almost identical broadenings for clusters of different sizes. Calculations with the Debye–Scherrer formula for the strongest (311) peak gave grain sizes of 6.4, 6.0, 5.8 and 5.2 nm for nanospheres with apparent sizes of 6.4 (a), 39.0 (b), 74.0 (c) and 191.0 (d) nm, respectively. This implies that the primary nanocrystals do not grow significantly with increasing size of nanospheres. The mechanism of nucleation and growth of the different porous sized SPION is evaluated. DEG can function as dual roles, i.e., a complexing agent and a solvent for the synthesis. It remains liquid in a wide range of temperatures (-10 to 245 °C) and has a high dielectric constant that enables the dissolution of polar and ionic substances. The unique chelating properties of DEG help to stabilize the complexed Fe³⁺, Fe²⁺ and Zn²⁺ in basic solution. DEA can function as activating agent for the sized-controlled synthesis. The metal DEG complexes undergo nucleophilic substitution reactions when the temperature or concentration of water in the system increased, which results in the condensation of mononuclear hydroxide reactive intermediates and eventually leads to precipitation of metal hydroxides or oxides (Scheme 1)¹⁸. It was noticed that the crystal diameter of sample was almost 5.5 nm, which indicated that DEA molecules may help to decrease the size of the Fe₃O₄ nanoparticles. With increasing DEA/DEG molar ratio from 1/4 to 1/1, the crystalline grain size of iron-oxide core increased sharply from 6.4 to 191 nm.

3.2 The magnetic properties of the different sized SPION

The unique and complex structure allows nanospheres to retain superparamagnetic behavior at room temperature even though their size far exceeds 20 nm. To evaluate the magnetic response of nanoparticles to an external field, the mass magnetization was

measured at room temperature by cycling the field between -5000 and 5000 Oe. Fig. 3 shows that all the nanoparticles are superparamagnetic at room temperature. The saturation magnetization of different sized nanoparticles was determined to be 67.01, 70.99, 75.53, and 81.84 emu g⁻¹ for nanospheres of 6.4, 39.0, 74.0 and 191.0 nm, respectively. Although the values are close for nanospheres of different size, it shows noticeable decrease for smaller particles, which may be attributed to the higher weight fraction of DEA in smaller particles or a surface related effect such as surface disorder. The magnetic moment μ of an individual grain can be determined by the Langevin paramagnetic function: $M(x) = N\mu[\coth(x) - (1/x)]$, where $x = \mu H/k_B T$, N is the number of clusters, H is the applied field, k_B is the Boltzmann constant, and T is the absolute temperature.

Fitting the data in Fig. 3 to this function, it is observed that magnetic moments for a single nanosphere of 6.4, 39.0, 74.0, and 191 nm are 8.45×10^{-17} , 3.23×10^{-14} , 1.79×10^{-13} and 7.13×10^{-13} emus, respectively. The dramatic increase in μ with increasing size (inset of Fig. 3) indicates that a single nanosphere would have a much stronger response to the external field than a single nanodot. As shown in inset of Fig. 3, the SPIONs are highly water dispersible (A), high magnetization (B) and superparamagnetic behavior (C).

3.3 The efficiency of DOX-Loaded SPION and In vitro DOX Release

To examine the drug delivery performance of porous SPION, DOX, an anticancer drug, was loaded into porous SPION with different diameter of 6.4, 39.0, 74.0 and 191.0 nm. The zeta potential measurements demonstrate that the Zeta potential values of relevant porous SPION are 31.5mV (6.4 nm), 28.8mV (39.0 nm), 26.4mV (74.0 nm) and 22.7mV (191.0nm), respectively. However, when SPION loaded with DOX and dispersed in medium (DMEM), the relevant Zeta potential values are -5.75mV (6.4 nm), -7.25mV (39.0 nm), -9.96mV (74.0 nm) and -12.3mV (191.0nm), respectively. The drug loading content and entrapment efficiency of DOX-SPION is shown in Table 1 and Fig. 4, respectively. The drug loading content was relatively higher for larger SPION containing more nanosphere cavity. The increase in drug loading content and entrapment efficiency was attributed to the increase in surface area from the porous SPION. The DOX-loaded SPION were well dispersed in the aqueous phase (Figure S1A), although the DOX-loaded SPION could be easily precipitated in the EP tube by centrifugation (Figure S1B). Figure 4 also shows the release profile of the drug from DOX-loaded porous SPION in PBS (pH 7.4) at 37°C. About 80% of the drug was released within 8 h by DOX-SPION (6.4 nm), while the release of DOX from the larger, porous SPION was not as fast as that from SPION (6.4 nm) and only about 55.1%, 47.9% and 42.4% of the loaded DOX was released from the different sized porous SPION carriers (39, 74, 191 nm) within 8 h, respectively. After 72 h the total percentage of the DOX released from the porous SPION drug carriers was about 70%. The porous DOX-SPION system obviously had a sustained release property, and its kinetics would thus be useful for cases that require a high initial dose followed by more stable release of smaller doses.

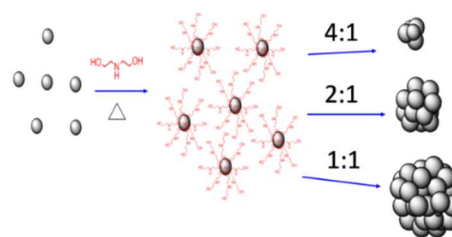
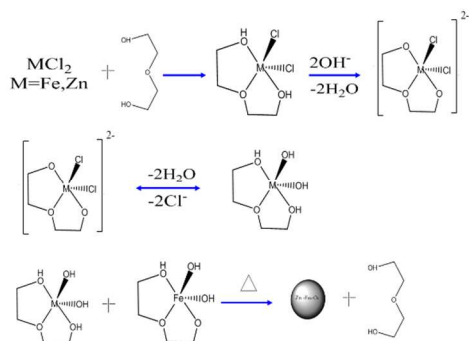
3.4 Cytotoxic effect of different sized SPION on HepG2 cells

The cytotoxicity of the carriers in the drug-delivery system has been also investigated in this study. Initially, the cytotoxicity effect of different sized porous SPION and DOX-loaded porous SPION on HepG2 cells were all characterized by MTT and Prussian blue exclusion assays. Fig. 5 shows cell viabilities against free DOX, DOX loaded porous SPION with different sizes. The concentration of drug-free porous SPION was set at the same level as that used in the group of DOX-loaded porous SPION. The results demonstrate that the cytotoxic efficacy of the DOX-loaded porous SPION and free DOX increases with the increasing drug concentrations, and the DOX-loaded porous SPION exhibit significantly greater cytotoxicity than free DOX. This may be attributed to the release of DOX inside cancer cells after efficient uptake of the DOX-loaded porous SPION in HepG2 cells (Fig. S2). Meanwhile, it can be seen from the cell viability study in Fig. 5 that porous SPION alone did not have a significant effect in cell viabilities after 48 h of incubation, indicating that porous SPION have relatively low cytotoxicity. This raises the possibility for the porous SPION to be utilized as promising candidates for potential drug loading and delivery into cancer cells to efficiently induce targeted cell death.

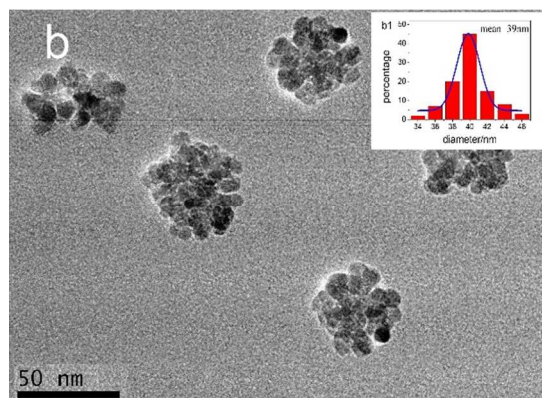
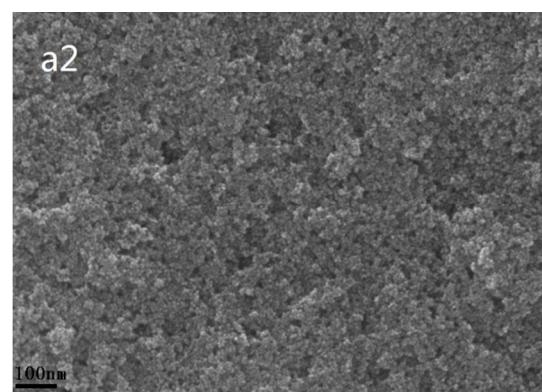
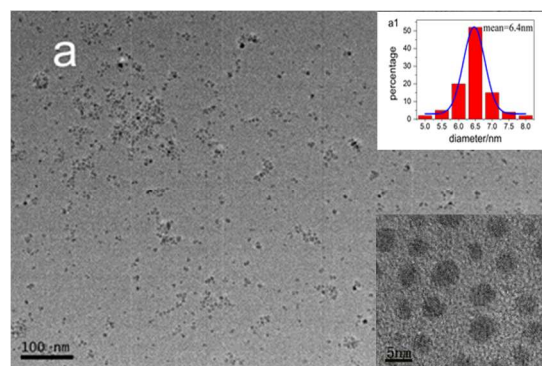
Inserting Graphics

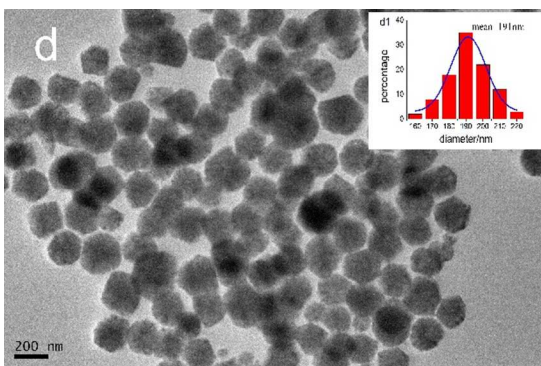
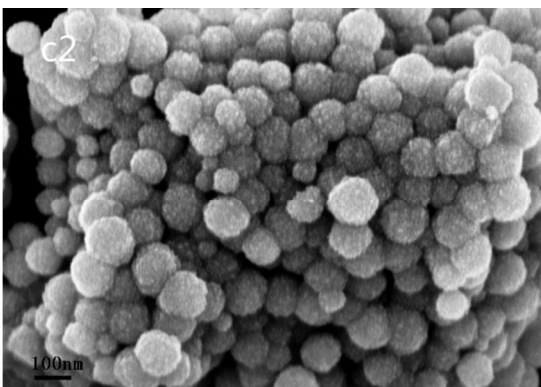
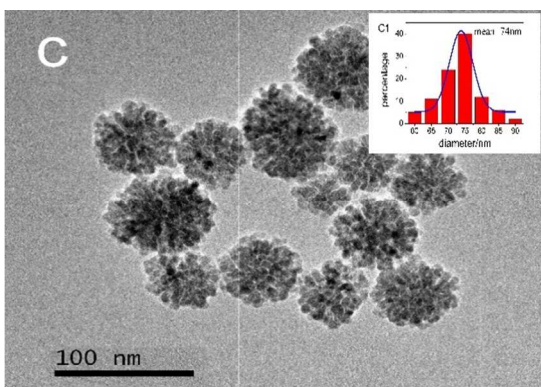
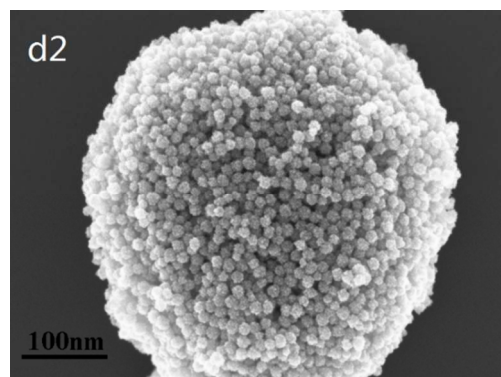
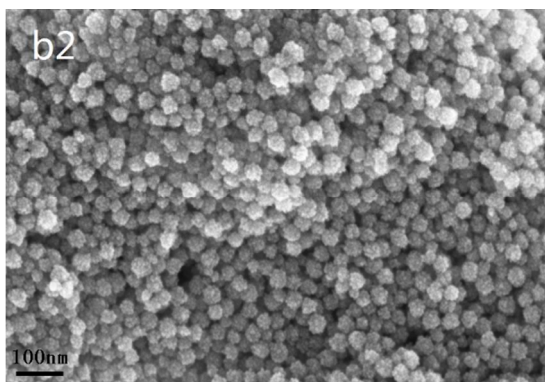
Table 1. The input amount of the reagents and the capacity of drug loading.

| Sample | DEG (mL) | DEA (mL) | Diameter (nm) | Drug loading capacity (%) | Encapsulation efficiency (%) |
|--------|----------|----------|---------------|---------------------------|------------------------------|
| a | 75 | 0 | 6.4 | 22.7 | 45.4 |
| b | 60 | 15 | 39 | 28.5 | 57.0 |
| c | 50 | 25 | 74 | 35.9 | 71.8 |
| d | 37.5 | 37.5 | 191 | 43.1 | 86.2 |



Scheme 1. Proposed scheme for complex formation and its hydrolysis in DEG solution and synthesis porous SPION by DEA. It was noticed that the different diameter (39 nm~191 nm) of samples could be synthesized with decreasing DEG/DEA molar ratio from 4/1 to 1/1, where the crystalline grain size of iron-oxide core is about 5.5 nm.





60

65

70

Fig.1. Characterization of the porous SPION: Transmission electron micrographs of porous SPION (a, b, c, d); Scanning electron microscopy of the porous SPION (a2, b2, c2, d2); Both size distribution histogram (column graph) and DLS measurement (blue curve) of porous SPION show their average diameters (6.4, 39.0, 74.0, 191.0 nm) (a1, b1, c1, d1).

80

85

90

100

110

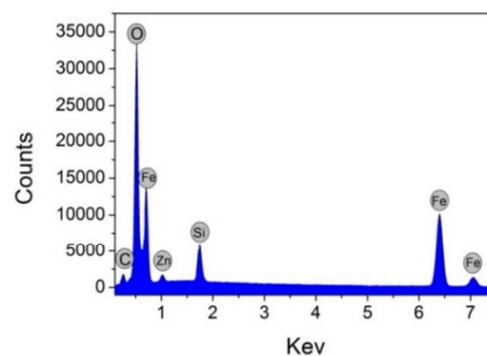
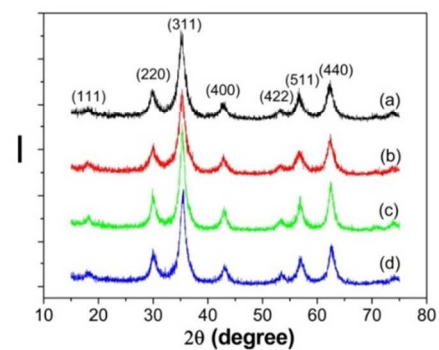


Fig.2. The powder X-ray diffraction patterns spectroscopy of porous SPION: 6.4 nm (a), 39.0 nm (b), 74.0 nm (c) and 191.0 nm (d) and the energy dispersive spectroscopy of porous SPION sample 6.4 nm (a).

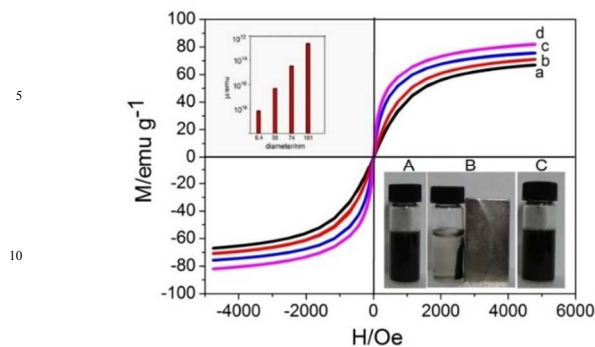


Fig.3. Hysteresis loops of SPION of 6.4 nm (a), 39.0 nm (b), 74.0 nm (c), and 191.0 nm (d). The upper-left inset shows magnetic moment μ per nanosphere (or dot) in a logarithmic plot. The lower-right inset shows photographs of an aqueous SPION dispersion in a vial without magnetic field (A), with magnetic field for 60 sec (B), and after the applied magnetic field is removed (C), indicating the good magnetic responsibility of SPION dispersed in water.

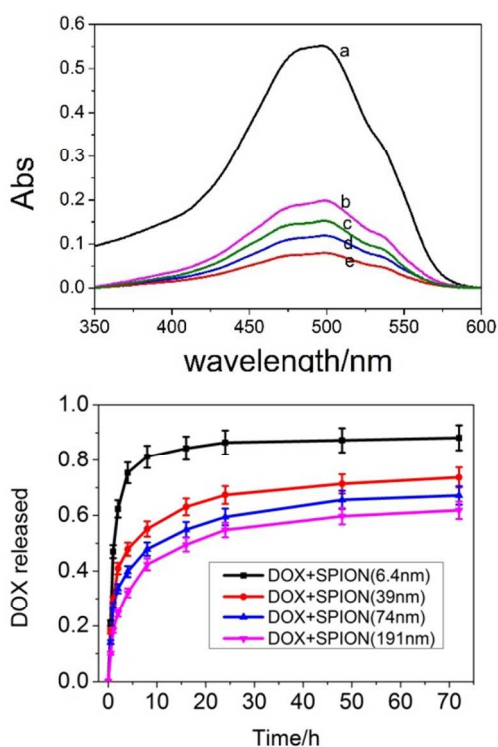


Fig.4. Loading capacity of DOX onto different sized of porous SPION in same initial DOX concentrations were measured of the supernatant by the UV absorption spectra of the DOX (a), DOX-SPION of 6.4 nm (b), 39.0 nm (c), 74.0 nm (d), and 191.0 nm (e), respectively. Release profile of DOX from DOX-loaded porous SPION in PBS at 37 °C.

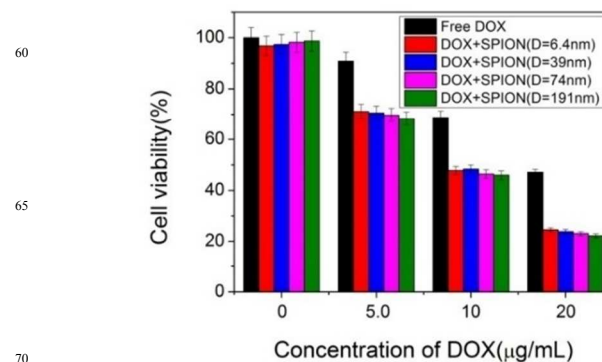


Fig.5. Cell viability of HepG2 cells treated with free DOX, DOX-SPION and free SPION for 24 h at different DOX concentrations. The cells treated with porous SPION alone (i.e., without loading DOX) show good cell viabilities (above 98%) after 48 h of incubation, indicating that porous SPION alone have relatively low cytotoxicity. In contrast, the DOX-loaded porous SPION exhibit significantly greater cytotoxicity than that without loading DOX.

4. Conclusions

In summary, we have explored the possibility for the synthesis of different sized porous SPION nanospheres ($Zn_{1/3}Fe_{8/3}O_4$) which are based on a new rational method of elevated-temperature hydrolysis of chelateiron alkoxide complexes in solutions of corresponding alcohol, DEG and DEA. The size of the SPION could be controlled by changing the ratio of the reaction medium. It is observed that the highly water dispersible porous SPION with narrow size distribution can be tuned from 6.5 to 200 nm, each of which is composed of many single magnetite crystallites approximately 5.5 nm in size. The nanospheres show superparamagnetic properties at room temperature. The SPION-induced cytotoxic effects on HepG2 cells demonstrate that different SPION porous spheres had no cytotoxicity after 48 h of incubation. The SPION porous spheres exhibited relatively fast cell uptake. DOX released from the SPION porous spheres had a sustained release pattern, and the DOX-loaded spheres exhibited greater cytotoxicity than free DOX, indicating its potential clinic application as ideal candidates for target drug delivery to realize efficient cancer diagnosis & therapy.

Notes

* State Key Lab of Bioelectronics (Chien-Shiung WU Laboratory), Southeast University, Nanjing 210096, P. R. China; E-mail: xuawang@seu.edu.cn

Acknowledgments

This work is supported by the National Basic Research Program (2010CB732404) and National Natural Science Foundation of China (81325011, 21175020, 21327902), the National High Technology Research and Development Program of China (863 Program) (No.2012AA022703)

References

1. G. P. Li and L. Q. Mao, *Rsc Adv*, 2012, **2**, 5108-5111.
2. J. Liu, Z. K. Sun, Y. H. Deng, Y. Zou, C. Y. Li, X. H. Guo, L. Q. Xiong, Y. Gao, F. Y. Li and D. Y. Zhao, *Angewandte Chemie-International Edition*, 2009, **48**, 5875-5879.
3. E. Natividad, M. Castro, G. Goglio, I. Andreu, R. Epherre, E. Duguet and A. Mediano, *Nanoscale*, 2012, **4**, 3954-3962.
4. A. P. Majewski, A. Schallon, V. Jerome, R. Freitag, A. H. E. Muller and H. Schmalz, *Biomacromolecules*, 2012, **13**, 857-866.
5. D. W. Qi, J. Lu, C. H. Deng and X. M. Zhang, *Journal of Physical Chemistry C*, 2009, **113**, 15854-15861.
6. Y. Pan, X. Du, F. Zhao and B. Xu, *Chemical Society Reviews*, 2012, **41**, 2912-2942.
7. F. Yan, L. Sun, F. B. Li, J. Q. Zhuang, H. L. Wang and W. S. Yang, *Journal of Nanoparticle Research*, 2011, **13**, 6613-6620.
8. B. Banerji, S. K. Pramanik, S. Mandal, N. C. Maiti and K. Chaudhuri, *Rsc Adv*, 2012, **2**, 2493-2497.
9. X. M. Zhu, J. Yuan, K. C. F. Leung, S. F. Lee, K. W. Y. Sham, C. H. K. Cheng, D. W. T. Au, G. J. Teng, A. T. Ahuja and Y. X. J. Wang, *Nanoscale*, 2012, **4**, 5744-5754.
10. J. Q. Wan, X. H. Jiang, H. Li and K. Z. Chen, *Journal of Materials Chemistry*, 2012, **22**, 13500-13505.
11. S. H. Sun, H. Zeng, D. B. Robinson, S. Raoux, P. M. Rice, S. X. Wang and G. X. Li, *Journal of the American Chemical Society*, 2004, **126**, 273-279.
12. M. L. Wen, Q. Li and Y. T. Li, *Journal of Electron Spectroscopy and Related Phenomena*, 2006, **153**, 65-70.
13. K. Zhang, Q. L. Liang, S. Ma, X. A. Mu, P. Hu, Y. M. Wang and G. A. Luo, *Lab on a Chip*, 2009, **9**, 2992-2999.
14. Wahajuddin and S. Arora, *International Journal of Nanomedicine*, 2012, **7**, 3445-3471.
15. V. I. Shubayev, T. R. Pisanic Ii and S. Jin, *Advanced Drug Delivery Reviews*, 2009, **61**, 467-477.
16. T. Sen, S. J. Sheppard, T. Mercer, M. Eizadi-Sharifabad, M. Mahmoudi and A. Elhissi, *Rsc Adv*, 2012, **2**, 5221-5228.
17. X. Yang, Y. Wang, X. Huang, Y. Ma, Y. Huang, R. Yang, H. Duan and Y. Chen, *Journal of Materials Chemistry*, 2011, **21**, 3448.
18. D. Caruntu, Y. Remond, N. H. Chou, M. J. Jun, G. Caruntu, J. B. He, G. Goloverda, C. O'Connor and V. Kolesnichenko, *Inorganic Chemistry*, 2002, **41**, 6137-6146.